Materials and Design 36 (2012) 714–727

Contents lists available at SciVerse ScienceDirect

Materials and Design

journal homepage: www.elsevier.com/locate/matdes

Technical Report

Effect of phase transformation and intermetallic compounds on the microstructure and tensile strength properties of diffusion-bonded joints between Ti–6Al–4V and AISI 304L

T. Vigraman [a], D. Ravindran [a,*], R. Narayanasamy [b]

[a] Department of Mechanical Engineering, National Engineering College, K.R Nagar, Kovilpatti 628 503, Tamil Nadu, India
[b] Department of Production Engineering, National Institute of Technology, Thiruchirappalli-620 015, Tamil Nadu, India

ARTICLE INFO

Article history:
Received 2 October 2011
Accepted 13 December 2011
Available online 19 December 2011

ABSTRACT

The occurrence of a phase transformation and the effect of intermetallic compounds on the microstructure and tensile strength properties of diffusion-bonded (DB) joints between Ti–6Al–4V and AISI 304L were studied in the temperature range of 875–950 °C with an interval of 25 °C, a bonding time of 60 min and pressures of 4 MPa and 8 MPa. A maximum tensile strength of 242.6 MPa, was observed for diffusion-bonded joints that were processed at a temperature of 900 °C, bonded for 60 min at a pressure of 4 MPa and annealed for 2 h at 750 °C. Optical microscopy and scanning electron microscopy (SEM) were used to examine the grain growth and the fine details of the interface structure. Energy dispersive X-ray analysis (EDAX) and X-ray diffraction analysis (XRD) revealed the existence of intermetallic compounds and corroborated the phase transformation.

1. Introduction

Titanium alloys (Ti-alloys) are light and strong and they possess good corrosion resistance properties that favour their usage in aerospace and corrosion resistance applications [1]. Among titanium alloys, Ti–6A–4V is the most widely used alloy for aerospace applications because of its low density, high strength, and high temperature properties. The cost of Ti-alloy is very high compared to that of stainless steels. The cost and material consumption could be reduced by bonding Ti–6Al–4V with AISI 304L, with or without an interlayer, to achieve the desired properties. Fusion welding is not suitable for joining advanced materials because it leads to the formation of hard and brittle phases at the welded region. Because of the limitations of fusion welding, diffusion bonding (DB) is more widely used to join dissimilar materials of two different species. The DB process is capable of joining all kinds of materials whose chemical and metallurgical properties are suitable for engineering applications.

Several authors have reported the feasibility of DB of dissimilar materials, with and without the use of interlayer materials, to improve their physical and metallurgical properties. Vigraman et al. [2,3] performed DB of dissimilar ferrous materials duplex stainless steel SAE 2205 with medium-carbon steel AISI 1035 and austenitic stainless steel AISI 304L to low-carbon steel with an interlayer material AISI 304L steel. The combined techniques of superplastic forming and DB of similar titanium alloys were investigated in the literature for the manufacture of advanced aircraft engine blades and heavy parts in an inert gas environment [4,5]. Xun and Tan [6] reported the application of combined superplastic forming and diffusion bonding to manufacture hollow engine blades. The low temperature superplastic properties were studied, and the production of hollow panel diffusion-bonded structures was reported in Ref. [7]. The effect of alloying elements on the microstructure of dual phase Ti-alloy subjected to superplastic deformation was published in Ref. [8]. Different diffusion bonding techniques were developed to bond pure titanium and Ti-alloys with several other metal combinations. The formation of diffusion-bonded joints between pure 'Ti' and pure 'Al' was reported by Wei et al. [9]. Titanium aluminide samples were diffusion-bonded with alternate layers of pure 'Al' and 'Ti' in another published work [10]. In a separate study [11], the use of a composite barrier layer for DB of TiAl to steel was reported. Konga et al. [12] conducted hot-pack roll bonding of Ti–6Al–4V with TiAl and obtained high bond strength for the diffusion-bonded joints. Kundu et al. [13,14] described the joint properties and microstructures of pure titanium diffusion bonded to austenitic stainless steel with a nickel interlayer. Torun and Celikyurek [15] performed the diffusion bonding of pure titanium with nickel under vacuum conditions and reported good bond formation; in addition, the highly polished DB samples were borided.

Yan et al. [16] performed vacuum hot-roll bonding of Ti-alloy and stainless steel using a nickel interlayer and obtained good

* Corresponding author. Tel.: +91 04632 222502; fax: +91 4632 232749.
E-mail addresses: tmvig.yanka@gmail.com (T. Vigraman), rmkv1@rediffmail.com (D. Ravindran), narayan@nitt.edu (R. Narayanasamy).

0261-3069/$ - see front matter © 2011 Elsevier Ltd. All rights reserved.
doi:10.1016/j.matdes.2011.12.024

tensile strength. The DB of Ti-alloy to stainless steel with an aluminium alloy interlayer was performed below the melting point of the aluminium alloy and reported by He et al. [17]. The interface microstructure and mechanical properties of DB joints between titanium and stainless steel with a niobium interlayer were studied by Kundu et al. [18]. The effect of the impulse pressure on the bonded samples between Ti-alloy and stainless steel was studied and presented by Yuan et al. [19]. Hot isostatic DB of Ti–6Al–4V and stainless steel (304 grade) was successfully performed and the joint strength was presented in the literature [20].

In the current work, direct DB of Ti–6Al–4V to AISI 304L was conducted by maintaining a vacuum at high temperatures and maintaining the surface finish requirements. The phase transformations that occurred at various temperatures and their effect on the tensile strength were studied. High pressures were applied prior to DB to plastically deform the surface asperities of the contact surfaces, finishing the surface and breaking the thin oxide layer formed after mechanical and chemical cleaning. The experimental evidence indicated the presence of intermetallic compounds at the interface and a phase transformation in the solid state. The diffusion-bonded joints exhibited brittleness and deleterious effects on strength of the joints when they were subjected to cyclic heating and cooling. However, the study was conducted to understand the phase transformations taking place at the joint region. This material combination could be used for corrosion resistance applications, but these joints should not be exposed to higher temperatures for longer duration.

2. Experimental details and processing

2.1. Materials

The chemical compositions of the Ti–6Al–4V and AISI 304L base metals are presented in Table 1. Rolled Ti–6Al–4V and austenitic stainless steel AISI 304L were purchased in the form of plates with thicknesses of 16 and 12 mm, respectively. The specimens were cut into $40 \times 40 \times 16$ mm pieces for the Ti–6Al–4V and $40 \times 40 \times 12$ mm for the AISI 304L. The mechanical strength of the base metals is provided in Table 2. The standard metallographic polishing technique with silicon carbide emery paper (up to 1200 grit) was used to obtain a mirror finish. The specimens were tested for surface roughness and centre line average (Ra) value. For Ti–6Al–4V, the Ra value was ±0.20 μm; for AISI 304L, it was ±0.32 μm. The flatness values of the Ti–6Al–4V and AISI 304L were ±8 μm and ±0.18 μm, respectively.

2.2. Equipment

The DB equipment consisted of a hydraulic press with a built-in vacuum furnace and an inert gas purging facility. Fig. 1a shows the DB specimen held between the two platens. The equipment is capable of bonding samples with diameters of 50 mm and thicknesses as high as 100 mm at a vacuum level of 50×10^{-4} Pa and the inert gas purging facility uses argon. The equipment is fitted with a linear scale to measure the axial strain with an accuracy of ±0.001 mm and a load cell to measure the applied load with an accuracy of ±25 N. The heating rate and cooling rate of the system can be controlled as required.

Table 2
Mechanical properties of the base metals.

Alloy	Yield strength (MPa)	Ultimate tensile strength (MPa)	Minimum elongation (%)
Ti–6Al–4V	896	960	11
AIS 304L	316	582.4	30

2.3. Procedure

DB experiments were conducted in the temperature range of 875–950 °C with an interval of 25 °C, a bonding time of 60 min and holding pressures set at 4 MPa and 8 MPa. The order of experiments and the parameter settings of the corresponding samples are listed in Table 3. Fig. 1b shows the DB sample with metallographic and tensile test specimens placed in the respective holes after they were subjected to the wire-cut electric discharge machining (WEDM) technique. From the DB samples, square metallographic specimens with dimensions of 8×8 and 6×6 mm and cylindrical tensile test specimens 4 mm in diameter and 28 mm in length (in accordance with ASTM standard E8M [21]) were cut from the bonded samples using a WEDM technique (shown in Fig. 1c). For optical microscopy, the specimens were polished with SiC emery paper with grit size up to 1200 and disc polished before etching. An Al_2O_3 slurry was used as an agent for disc polishing. Chemical etching was performed on the Ti–6Al–4V side in two stages. First, it was etched with a solution of 8 ml HF, 10 ml HNO_3 and 82 ml H_2O, followed by 18 g/l of NH_4HF_2 in H_2O to identify different phases and measure grain size and surface defects. The AISI 304L regions were etched with a solution of 10 ml HNO_3, 10 ml acetic acid, 15 ml HCl and two drops glycerol. The microhardness values were measured by applying a load of 25 g in the direction transverse to the bond line. Energy dispersive X-ray analysis (EDAX) was performed at various points in the transverse direction, starting from one base metal to another across the interface of the bonded samples. Scanning electron microscopy (SEM) and X-ray diffraction analysis (XRD) measurements of the samples were conducted with a diffractometer system to determine the reaction products at the joint region.

2.3.1. Effect of heat treatment

In addition, the bonded samples were subjected to an annealing heat treatment for 2 h at 750 °C to study its effect on their phase kinetics and strength. The tensile test samples and metallographic specimens were cut and prepared for testing, as explained in Section 2.3. The SEM, EDAX and XRD analyses were then performed on selected samples.

3. Results and discussions

3.1. Optical microscopy

Fig. 2a and b shows the as-received base metal microstructures of AISI 304L and Ti–6Al–4V, respectively. The grain sizes of the bonded materials (16 μm for AISI 304L and 10 μm for Ti–6Al–4V, both processed at 950 °C) are larger than those of the as-received materials (AISI 304L 7 μm and Ti–6Al–4V 8 μm) because of grain growth during the bonding process at higher

Table 1
Chemical composition of the base metals (weight%).

Alloy	C	Mn	Si	S	P	Cr	Ni	Mo	Cu	V	Al	Fe	Ti
Ti–6Al–4V	0.02	–	0.03	–	–	0.02	0.01	0.03	–	4.31	6.58	0.18	Bal.
AISI 304L	0.01	1.54	0.36	0.03	0.04	18.3	8.38	0.59	0.75	0.06	–	Bal.	–

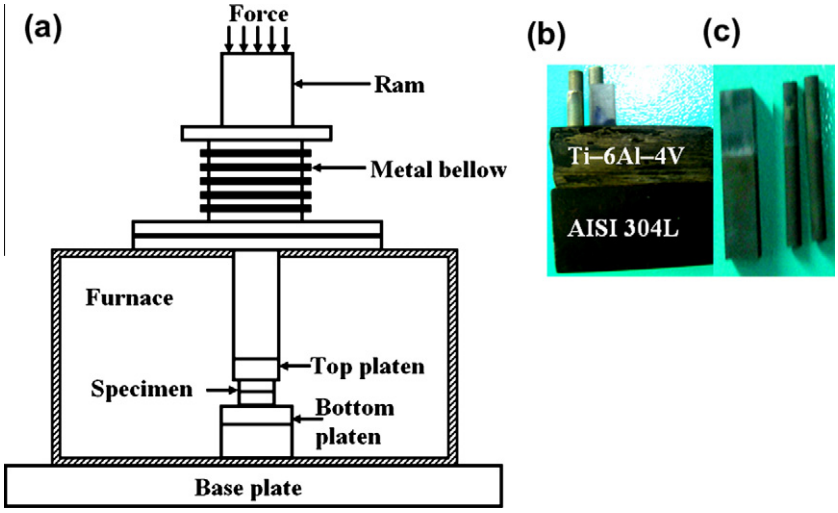

Fig. 1. (a) The joint assembly, (b) diffusion-bonded sample with wire-cut specimens, (c) wire-cut metallographic and tensile test specimen.

Table 3
The parameter settings for the experiments.

Specimen name	Process parameters (°C/MPa/Min.)	Heat treated specimen name
S1	875, 8, 60	S1H
S2	950, 4, 60	S2H
S3	900, 8, 60	S3H
S4	925, 4, 60	S4H
S5	925, 8, 60	S5H
S6	900, 4, 60	S6H
S7	875, 4, 60	S7H
S8	950, 8, 60	S8H

Note: °C – represents temperature, Min – represents holding time and Mpa – represents applied pressure. S1H – S8H-DB specimens were annealed for 2 h at 750 °C.

temperatures and during the subsequent annealing. The insert micrograph in Fig. 2a shows twin bands of annealed austenite grains (γ-phase) in the AISI 304L steel. In Fig. 2b, the insert in the right top corner shows the presence of columnar grains along the rolling direction of the Ti–6Al–4V alloy. Because Ti–6Al–4V is a binary phase alloy, the insert in Fig. 2b shows an equiaxed alpha ('α' light in colour) phase with an intergranular beta ('β' dark in colour) phase. Carbide precipitation along the grain boundaries is noted in the base metal AISI 304L regions of all of the diffusion-bonded samples, as noted in Fig. 2c. In addition, grain matrix carbide precipitation is observed and also shown in Fig. 2c. Tan et al. [22] reported that grain growth was very high in the temperature range of 700–800 °C for Ti–6Al–4V under strain, and it was slow in between 850 and 950 °C. In the current study, grain growth in the Ti–6Al–4V alloy region (diffusion-bonded base metal) after DB is insignificant in the temperature range from 800 to 900 °C because recrystallisation of the beta phase caused resistance to grain growth. This behaviour is in agreement with reports in the literature [23]. Fig. 2d shows the beta ('β') phase surrounding the alpha ('α') grains in the microstructure of the Ti–6Al–4V base metal. Here, the grain growth of the 'α' phase is inhibited by the 'β' phase, which pins down the grain boundaries. The effect of annealing on Ti–6Al–4V has been reported by Kim et al. [24]. In Fig. 2a, a net-work of elongated small and coarse grains can be seen in the as-received AISI 304L steel. Fig. 2b shows an equiaxed microstructure with a nearly even distribution in the as-received Ti–6Al–4V alloy. After the DB process at 950 °C, a region (away from the interface) exhibits a pattern that is characteristic of the Widmanstatten structure.

Fig. 3a–d shows the micrographs of DB samples S1, S4, S6 and S8, processed at different temperatures (see Table 3). Generally, as the DB temperature increases, the rate of interface reaction also increases. This increase occurs because more complex intermetallic compounds form at the interface as a result of the diffusion of various elements across the interface. These micrographs reveal good bonding between the Ti–6Al–4V and AISI 304L. The width of the reaction zone at the joint interface increases as the bonding temperature increases. A narrow width of 3–4 μm is observed for the S1 samples in Fig. 3a, as identified in Table 3. The width of the reaction zone increases to 8–10 μm, 10–12 μm, and 14–16 μm for the samples S4, S6 and S8, respectively (Fig. 3b–d). In Fig. 3a–c, the presence of 'α' and 'β' rich regions closer to the interface is noted. In the adjacent areas near the interface on both sides of the base metal, grain growth is observed. This growth occurs as a result of diffusion of elements from the base metal to the interface. In the absence of these elements in the form of carbides or precipitates, the grain boundaries cannot be pinned down at elevated temperatures. Therefore, grain growth takes place (refer Fig. 3b). In the non-heat-treated (unannealed) samples shown in Fig. 3, the amount of the 'β' phase observed is high compared to the amount in the annealed samples.

In addition, fine grains occur at the interface (see Fig. 3c and d). In the AISI 304L base metal region, carbide segregation is observed along the grain boundaries. A bright line occurs at the interface in Fig. 3d, which indicates presence of various intermetallic compounds. The formation of intermetallic compounds was confirmed by referring to literature reports [25,26].

Post-heat-treatment annealing was performed on the DB samples; the optical microstructures of the samples S1H, S4H, S6H and S8H (see Table 3) are shown in Fig. 4a–d. Fig. 4a–d shows that as the DB temperature increases grain growth is observed adjacent to the grain boundaries. With the increase in the DB temperature, the grain size increases in the AISI 304L base metal adjacent to the reaction zone and the width of the reaction zone increases. The high-temperature thickening of the reaction zone occurs because of the formation of hard, stable intermetallic compounds at the interface. The measured width of the reaction zone for samples S1H, S4H, S6H and S8H increases to approximately 20–24 μm, 38–44 μm, 36–42 μm and 46–51 μm, respectively, as shown in Fig. 4a–d. In Fig. 4a, the width of the reaction zone increases because of the annealing heat treatment performed on sample S1H.

On the Ti–6Al–4V side, grain growth is also observed at higher DB temperatures. With increasing DB temperature, the amount of

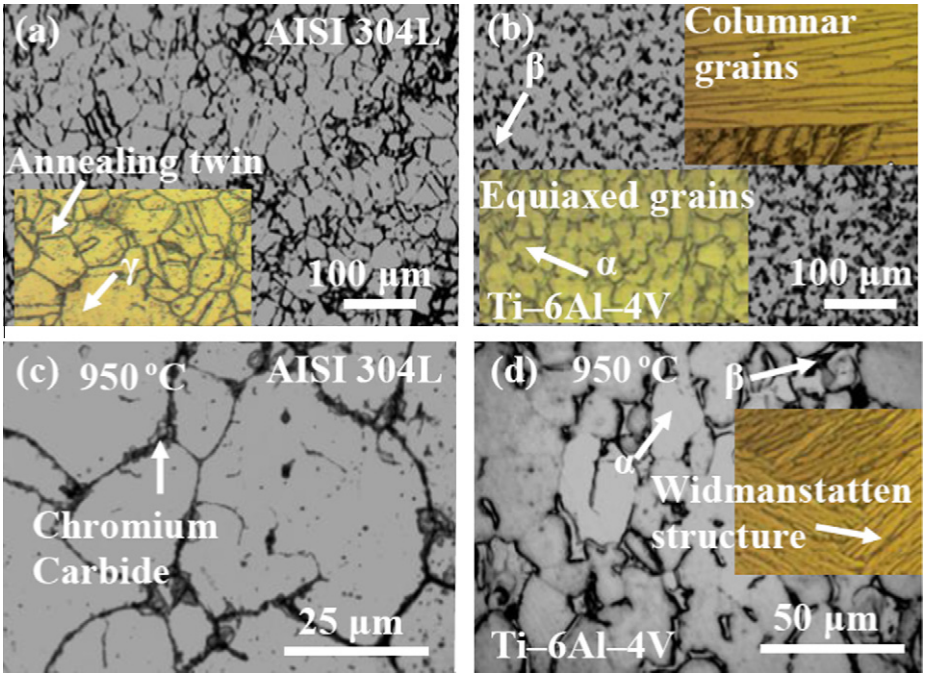

Fig. 2. Base metal microstructures: (a) as-received AISI 304L, (b) as-received Ti–6Al–4V, (c) DB sample heat-treated AISI 304L and (d) DB sample heat-treated Ti–6Al–4V.

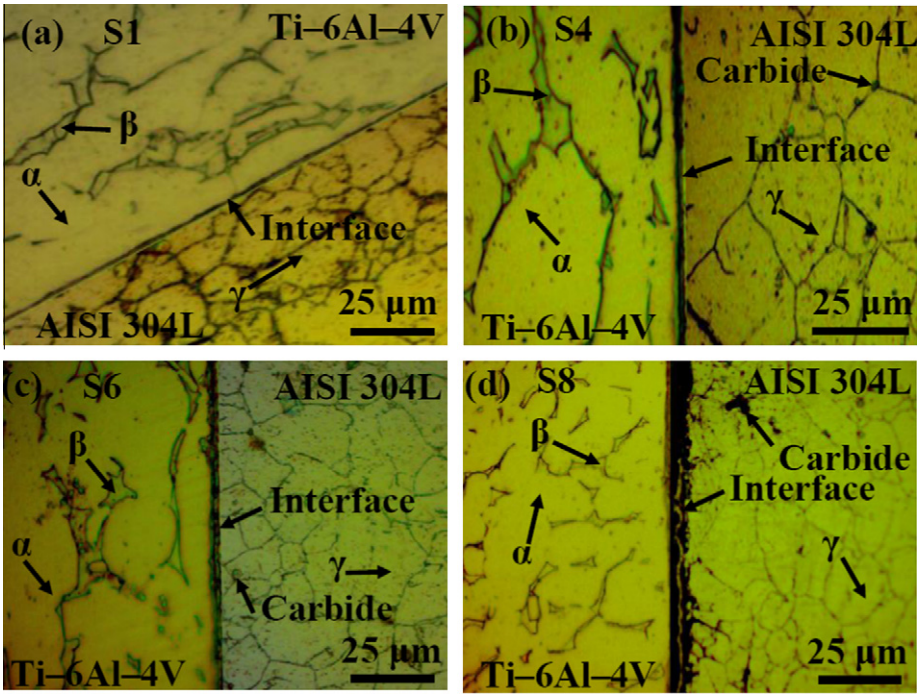

Fig. 3. (a–d) Optical micrographs of diffusion-bonded samples with various process parameters.

the 'β' phase on the Ti–6Al–4V side increases near interface because of the diffusion of β-stabilizing elements, namely, 'Fe', 'Cr', 'Ni', 'Mn' and 'Si' from the AISI 304L region. However, the presence of the 'β' phase near the interface is masked, and it cannot be seen clearly because the etchant spills onto the Ti–6Al–4V side and masks the 'β' phase while etching the AISI 304L side.

The thickness of the interface reaction zone increases at higher temperature because of the diffusion of 'Ti', 'Al' and 'V' into the AISI 304L regions. The diffusion of elements from both base metals across the interface enables the formation of binary, ternary or mixed binary and ternary compounds at the interface.

In Fig. 4b, the width of the reaction zone is uniform over the length of the joint. Closer to the interface, fine grains of intermetallic compounds and the needle-like 'β' phase are observed. In general, carbide segregation occurs at the grain boundaries (refer to Fig. 4b) in the base metal AISI 304L region. In the Ti–6Al–4V base metal, away from the interface, both the 'α' and 'β' phases are seen in Fig. 4c. Near the interface in the AISI 304L base metal, a

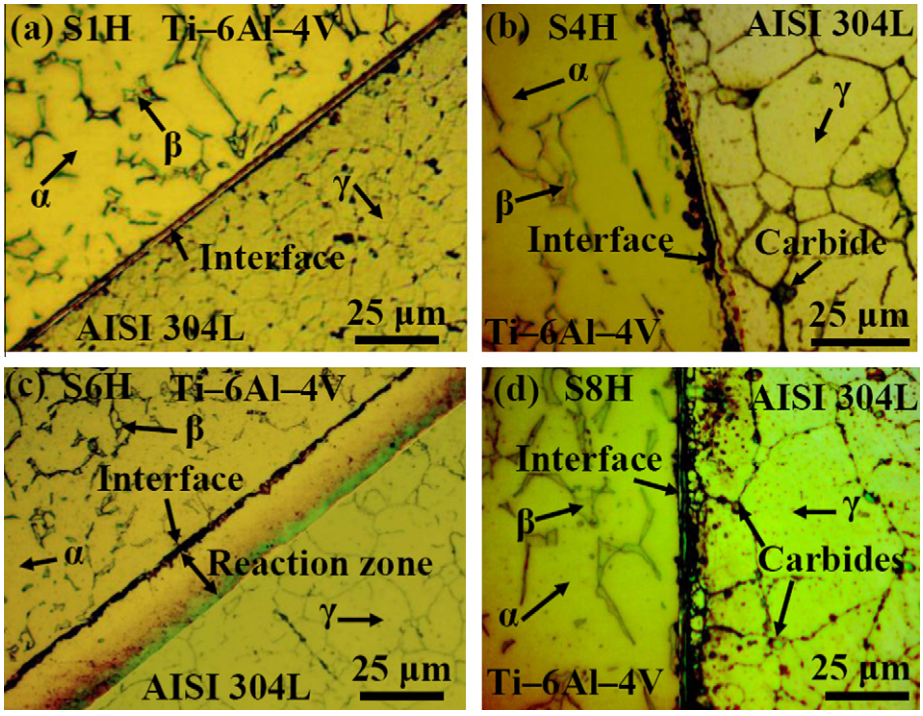

Fig. 4. (a–d) Optical micrographs of the bonded samples subjected to annealing heat treatment.

thick-banded region occurs, which is rich with diffused elements. In addition, the reaction zone in sample S6H is wider than the corresponding zones in SIH, S4H and S8H.

In Fig. 4b and d, the base metal Ti–6Al–4V region near the interface contains dark-coloured compounds, which may be intermetallic compounds and carbides. Because 'Ti' has higher diffusivity than 'V', a greater amount of TiC may be formed than vanadium carbide. The formation of TiC and VC pins the grain boundaries in the interface. All of these factors contribute to the fine-grained microstructure that is obtained at the interface. In both cases, the formation of several intermetallic compounds at the interface increases the width of the interface reaction zone. In all of the above samples, heat treatment annealing was performed at 750 °C for 2 h. After the heat treatment, improved interfacial strength is expected as a result of increased atomic diffusion across the interface.

The annealing heat treatment reduces the amount of the 'β' phase present in the Ti–6Al–4V near the interface because 'Ti', 'Al' and 'V' diffuse into the AISI 304L region. Consequently, stronger and more stable intermetallic compounds are formed at the interface, and the thickness of the interface increases. Because titanium carbides and vanadium carbides are fine-grained and smaller in size than FeC, CrC or ternary carbides, they appear brown in colour at the interface. Vanadium also has strong chemical affinity towards carbon; as a result thermodynamically stable VC is formed.

The thickness of the reaction layer varies because of surface asperities. This variation is shown in Fig. 5a and b for samples that were subjected to large pressures (in the range of 20–30 MPa) from the beginning of heating up to a temperature of 750 °C. In this case, the processing temperature was 925 °C. During DB, surface asperities deform plastically at the mating surfaces, as shown in Fig. 5a, and a thick, wavy interface is produced. The waviness of the interface is caused by plastic deformation of the surface asperities during bonding. The interface appears thick in locations where diffusion is increased and more intermetallic compounds are formed as a result of the increased contact area in localised pressure zones that formed during diffusion bonding. Therefore, the thickness of the interface is not uniform over its length. The variation in the thickness of the reaction zone is of the order of 17–39 μm for samples processed at 925 °C (see Fig. 5a). A highly finished flat surface induces even diffusion of atoms across the interface over the length, producing a reaction zone of uniform thickness (see Fig. 5b, sample processed at 925 °C).

3.2. SEM micrographs

Fig. 6a–d shows the SEM images of the non-heat-treated samples SI, S4, S6 and S8 (refer to Table 3). As shown in Fig. 6a, the interface appears thin and straight over its length. The magnified microstructure reveals the presence of discontinuities, voids and intermetallic compound formation. Further, a fine fragmented 'β'

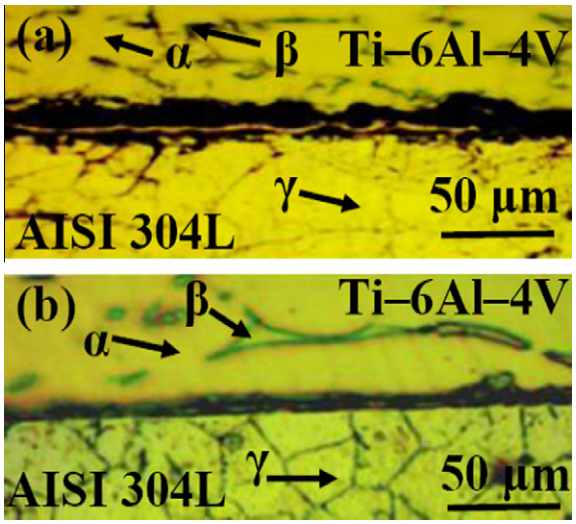

Fig. 5. (a) and (b) Representative microstructures revealing effect of surface asperities.

phase is observed adjacent to the interface in the Ti–6Al–4V region. The appearance of this phase is in accordance with the observations made in other studies [27,28]. From the SEM micrographs, it is evident that the increase in the joining temperature increases the diffusion of chemical species across the interface, leading to an increase in the width of the diffusion zone. In Fig. 6a, a thin dark region that is rich with 'β' phase and a mixture of intermetallics can be seen at the interface. Adjacent to that, a region rich with FeTi, Fe_2Ti, Ni_4Ti_3 and other intermetallic compounds is observed in the Ti–6Al–4V base metal closer to the interface. The presence of the 'β' phase, FeTi and Fe_2Ti closer to the interface is confirmed by the reported work of Kundu et al. [28].

Fig. 6b reveals that the formation of a thicker interface is caused by the increased thermal diffusivity at 925 °C. In the interface, the 'σ' phase, carbides such as TIC and VC and other intermetallic compounds are observed (see the magnified image). Adjacent to the darkly shaded region (see Fig. 6b), a lightly shaded region occurs, which indicates the presence of titanium aluminide (Ti_3Al). Titanium aluminides form because of the diffusion of 'Al' atoms towards the AISI 304L, which raises the concentration of 'Al' adjacent to the interface above 5.5%. As a result, the above-mentioned compounds are formed. Salishchev et al. [29] has reported the formation of sub-microcrystalline titanium aluminides, which are similar to the crystalline structure obtained near the interface in the present work, by hot working. Compared to Fig. 6a, Fig. 6b shows a thick layer of a white phase at the interface on the Ti–6Al–4V side. This result indicates the presence of the 'β' phase at the interface, which occurs as a result of diffusion of β-stabilizing elements at increased temperature (925 °C). At the interface region, a smaller white intermetallic compound is found, which may be TiNi or Ti_2Ni. Fig. 6c reveals the presence of a smaller and thinner interface than that in Fig. 6b as a result of the lower processing temperature 900 °C. The SEM image of sample S6, shown in Fig. 6c, indicates the presence of the 'β' phase at the grain boundaries of the 'α' grains. A dark grain adjacent to the interface reveals the presence of crystalline compounds which are identified as Ti_3Al by referring to the work performed by Liauo et al. [30]. Lightly shaded regions are also observed, indicating the presence of TiAl, and Ti_3Al (see Fig. 6c). These phases were identified by referring to the report by Feng et al. [31]. In the base metal AISI 304L, austenite grains and grain boundaries are clearly visible (see Fig. 6d), and spherical carbides are present in some places at the grain boundaries. These carbides, of the $(Fe, Cr)_{23}C_6$ type, possess a more regular shape than other observed titanium carbide. At the interface, the 'σ' phase, TiNi, Ti_2Ni and other intermetallic compounds occur. In contrast to Fig. 6a, there is no line of discontinuity, and the interface appears to be thin. The interface seen in the insert in Fig. 6c is completely diffused, without any voids. This region may contain 'β' phase, intermetallic compounds specifically Fe_2Ti, FeTi, Ni_4Ti_3, TiAl and Ti_3Al.

As shown in Fig. 6d, the fragmentation of the 'β' phase occurs close to the interface, on the Ti–6Al–4V side. The interface appears to be thick as a result of the formation of several intermetallic compounds. The elongated black layer indicates the presence of 'σ' and 'Fe', 'Cr' and 'Ni' rich intermetallic compounds. The thick white layer indicates the additional presence of TiNi, Ti_2Ni and the 'β' phase at the interface.

Fig. 7a–d shows interfacial SEM images of the samples annealed at 750 °C for 2 h, processed at different DB temperatures (see Table 3). It is generally observed that the increasing DB temperature also increases the width of the interface in comparison to Fig. 6, indicating that the width increases because of the 750 °C annealing. During annealing, thermal diffusion causes the formation of increased amounts of intermetallic compounds, increasing the width of the interface. In the heat-treated samples, the amount of 'β' increases because of the diffusion of 'β'-forming elements into the Ti–6Al–4V side from the AISI 304L.

As shown in the magnified image in Fig. 7a a white layer of carbides is found in addition to the other intermetallic compounds and the 'σ' phase. A line of discontinuity (elongated void) is also observed in Fig. 7a because of the lack of diffusion at the processing temperature of 875 °C. However, the width of the void or line of discontinuity decreases in comparison to the non-heat-treated sample (see Fig. 6a). The area in the circle is shown at higher magnification on the right side of Fig. 7a, revealing an elongated phase of TiAl compound, pointing towards the interface. Titanium aluminides form closer to the interface in the Ti–6Al–4V and at the interface because of the migration of 'Al' atoms towards the AISI 304L. As the 'Al' concentration increases beyond 5.5% at the interface, the formation of such compounds occurs. This observation is in good agreement with the observations made in the literature [32]. At the interface, intermetallic compounds such as 'σ', FeTi, Fe_2Ti, $TiCr_2$, Al_4CrNi_{15}, TiAl and Ni_4Ti_3 are present. The presence of these compounds is confirmed by the XRD analyses performed on that region.

At higher DB temperatures, a thick interface reaction zone is observed in Fig. 7b. In the magnified image (Fig. 7b), twisted bands of different intermetallic compounds are observed. These bands are particularly evident in the annealed samples because of the migration of the interface. These bands are oriented at approximately 45–50° with respect to the interface and parallel to each other. They appear as alternate bands of black and white that form different compounds at the interface. Moreover, they overlap the interface as they form because of the diffusion of atoms at the annealing temperature of 750 °C.

As shown in Fig. 7c and d, the fragmentation of the 'β' phase takes place at higher bonding temperatures. In Fig. 7c, the width of the interface decreases compared to that in Fig. 7b because the DB temperature is lower. Further, as mentioned earlier, all types of intermetallic compounds are observed at the inseparable interface. When the DB temperature is raised to 950 °C, as shown in Fig. 7d, a cellular band of structure is observed. This band indicates the presence of increased amounts of intermetallic compounds, including 'σ' and other phases. The presence of this type of cellular structure may reduce the strength of the interface because of the presence of various intermetallic compounds. Dynamic recrystallisation could explain the formation of the cellular structure. This explanation is in good agreement with the reported literature [33,34]. In general, the DB samples that are processed at higher temperatures and subjected to annealing heat treatment tend to undergo phase transformations leading to the formation of increased amounts of intermetallic compounds, such as 'σ', 'FeTi', 'Fe_2Ti', Ni_4Ti_3, Ti_2Ni, Ti_3Al and TiAl.

3.3. EDAX examination

The EDAX analysis shown in Fig. 8a and b, performed at points '3' and '4', corresponds to the sample S6, as described in Table 3. The diffusion of elements, such as 'Fe', 'Ni', 'Cr' and 'Mn', into the Ti–6Al–4V region is noted (indicated by the circle in Fig. 8a). The presence of these elements at a point indicates the formation of Fe_2Ti, TiNi, Ti_2Ni, and Al_4CrNi_{15}. The binary phase diagram indicates that the solubility of Fe (0–0.047%) in the 'α' phase is less than its solubility (0–24.7%) in the 'β' phase. In addition, at the reaction zone close to the interface, the concentration of 'Al' and 'V' is elevated leading to the formation of compounds such as TiAl, Ti_3Al, Fe_2V_3 and Al_6Ti_{19}. The presence of these compounds is confirmed by the XRD measurements taken at the joint region. As shown in Fig. 8b, at the AISI 304L region, the diffusion of elements such as 'Ti', 'Al' and 'V' is observed in the reaction zone adjacent to the interface. The diffusion of 'Ti', 'Al' and 'V' into AISI 304L side promotes the formation of intermetallic compounds with elements such as 'Fe', 'Cr', 'Ni' and 'Mn'. The various elements exhibit substitution diffusion mechanism. This means that exchange of atoms takes place in vacant sites. Vacant sites are created because

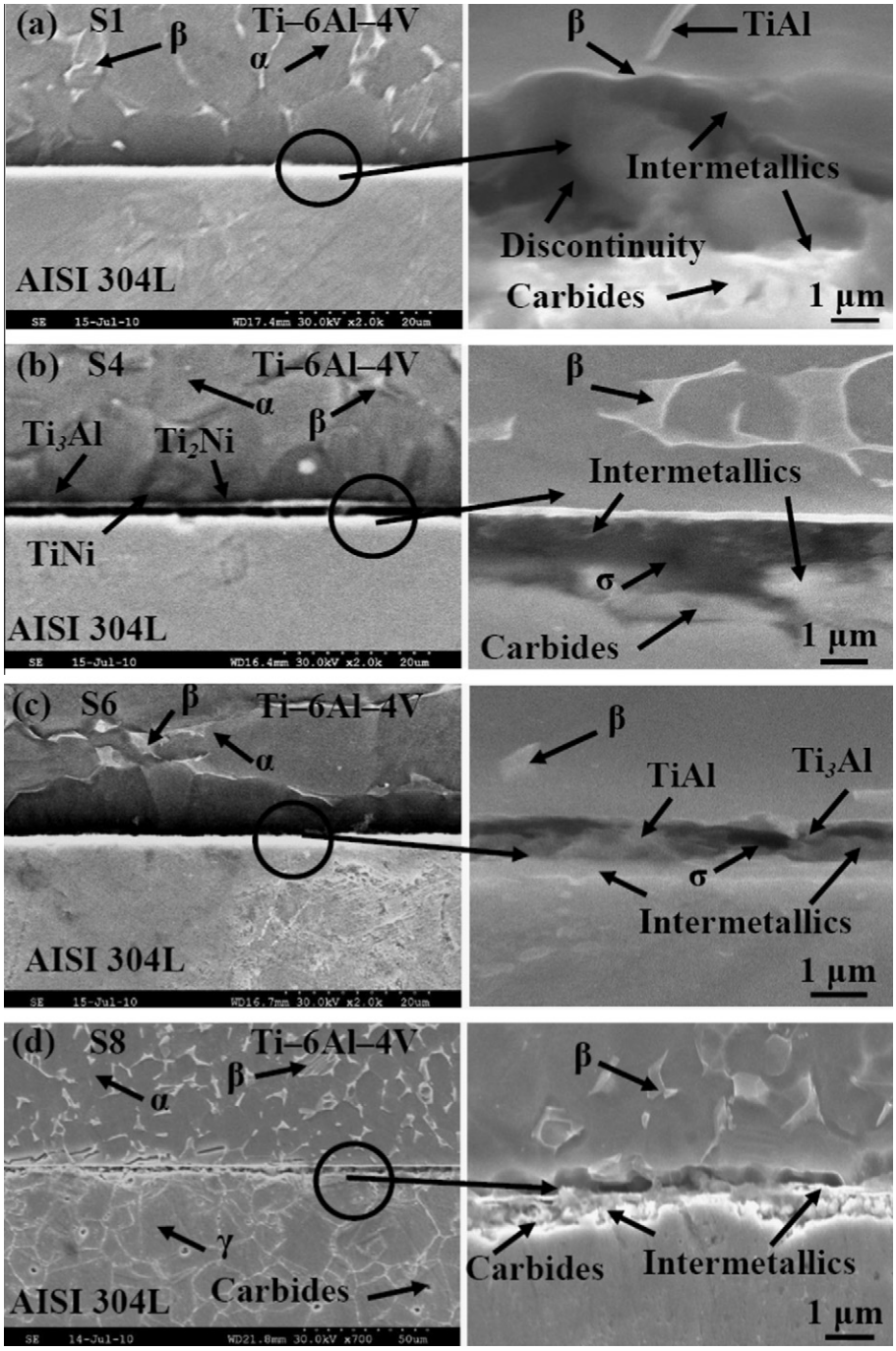

Fig. 6. (a–d) SEM images with inset of the diffusion-bonded samples with various process parameters.

of jump of atoms when the samples are raised to higher temperature. Further, the diffusivity of these elements across the interface takes place because of chemical potential difference. The formation and presence of compounds such as 'σ' (a mixture of 42.7–48.2% Cr + Fe + Ni + Ti), Fe_2Ti (68.2–75.4% Fe + bal. Ti), Mn_2Ti, $TiSi_2$ (54% Si + bal. Ti) and $AlNi_2Ti$ are observed with EDAX analysis. During bonding between Ti–6Al–4V and AISI 304L, 'Ti' diffuses more deeply into the austenitic stainless steel. The formation of 'σ' and carbides were confirmed in the published work of Voort et al. [35]. The migration of 'Cr' towards the interface produces a 'Cr' rich region along the interface in the AISI 304L base metal, which causes the formation of the 'σ' phase. The above phases are identified by the results of the XRD report and confirmed with the phase diagrams drawn between 'Cr' and 'Ti' by Murray [36]. The EDAX results and binary phase diagrams corroborate the claim that the 'σ' phase is a mixture of 'Fe', 'Cr', 'Ni', and 'Ti'. In addition, the presence of small quantities of carbides in that region is noted. These carbides can be either TiC or VC because 'Ti' and 'V' have higher chemical affinity for 'C' than for 'Fe' or 'Cr'. In the base metal AISI 304L, carbides of the $(Fe, Cr)_{23}C_6$ type carbides are observed at the grain boundaries. These two types of carbides differ in the following way: TiC is grey in colour and possesses a less regular shape, but $M_{23}C_6$ carbides are dark in colour and more regular in shape.

The solubility of 'Cr' is 0–0.2% in the 'α' phase and 0–100% Cr in the 'β' phase. Therefore, 'Cr' promotes the formation of the 'β' phase, and possibly the formation of 'γ'-$TiCr_2$ and Al_4CrNi_{15} closer

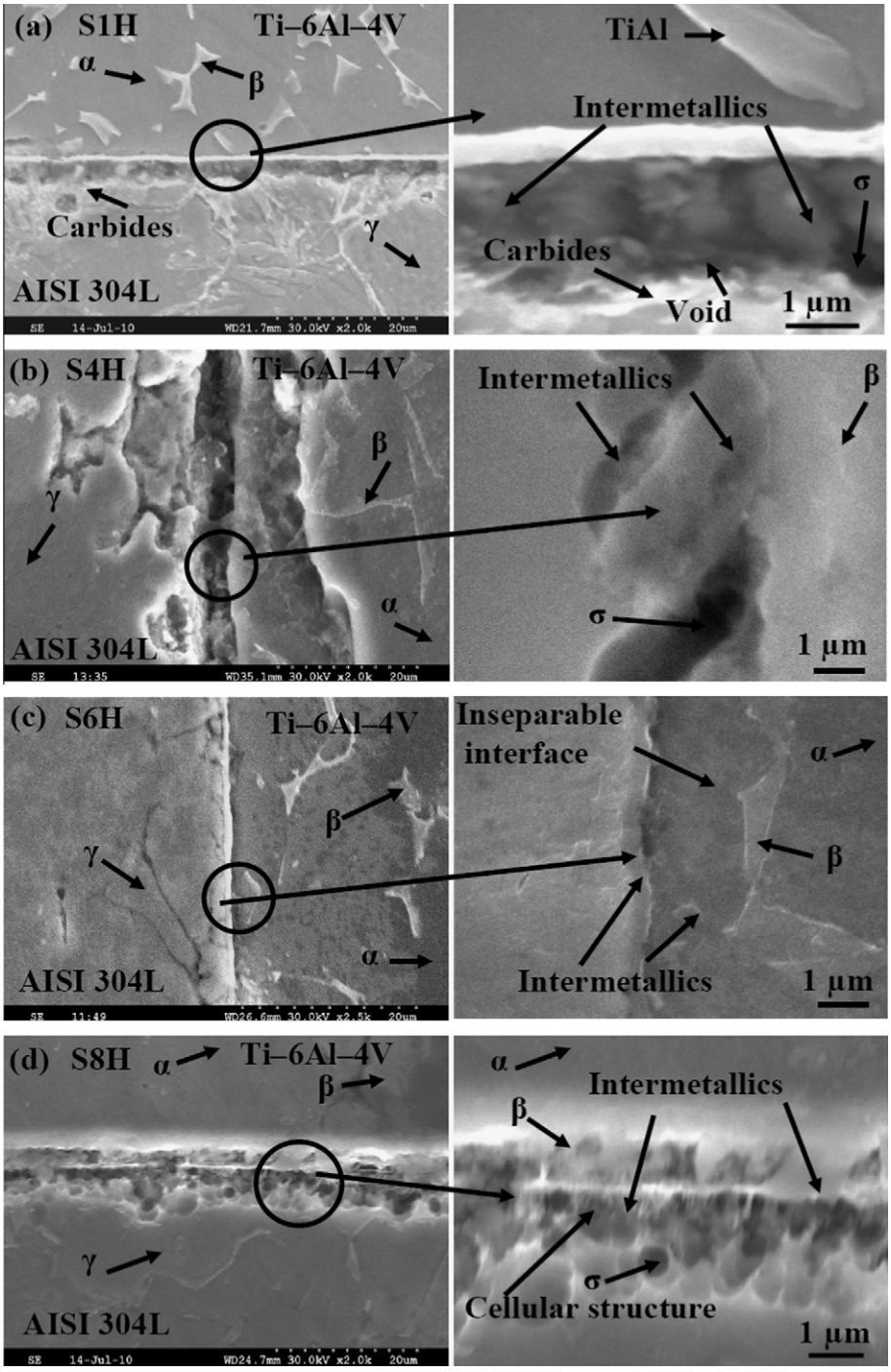

Fig. 7. (a–d) SEM images with inset of the bonded samples subjected to annealing heat treatment.

to the interface in the annealed samples. The phase diagram drawn between 'Cr' and 'Ti' by Murray [36] confirms the presence of these phases. The phases were also identified by referring to the reported literature [37,38]. The solubility of 'Si' is limited (0–0.3% Si) in the 'α' phase and 0–2.1% Si in the 'β' phase, as mentioned in the phase diagram drawn between 'Si' and 'Ti' by Murray [39]. AISI 304L contains only 0.36% Si; however, the 'Si' concentration increases closer to the interface, and $TiSi_2$ is formed. This increased concentration indicates that the diffusion of 'Si' towards the interface is thermal activation oriented. The thermal energy creates vacancies because of jump of atoms. These vacancies would be occupied by the diffused atoms. In this case, the 'Si' atom occupies the vacancies.

The EDAX analysis of annealed sample S8H is shown in Fig. 8c and d. EDAX was performed at points '3' and '4', which are marked in the embedded SEM image. At point '3', the presence of Fe_2Ti, Ni_4Ti_3, $Fe_3Al_2Si_4$, Al_6Ti_{19}, and Fe_2Ti_4O is noted. The presence of oxides in the joint region of the annealed samples is attributed to difficulty in maintaining the vacuum environment during annealing. The growth of hard brittle phases on either side of the joint is noted from the EDAX results. The presence of Ni_4Ti_3 in the interface indicates the diffusion of 'Ni' from the AISI 304L side and 'Ti' from the Ti–6Al–4V region towards the interface. This phase identification was performed by referring to the phase diagram drawn between 'Ni' and 'Ti' by Murray [39].

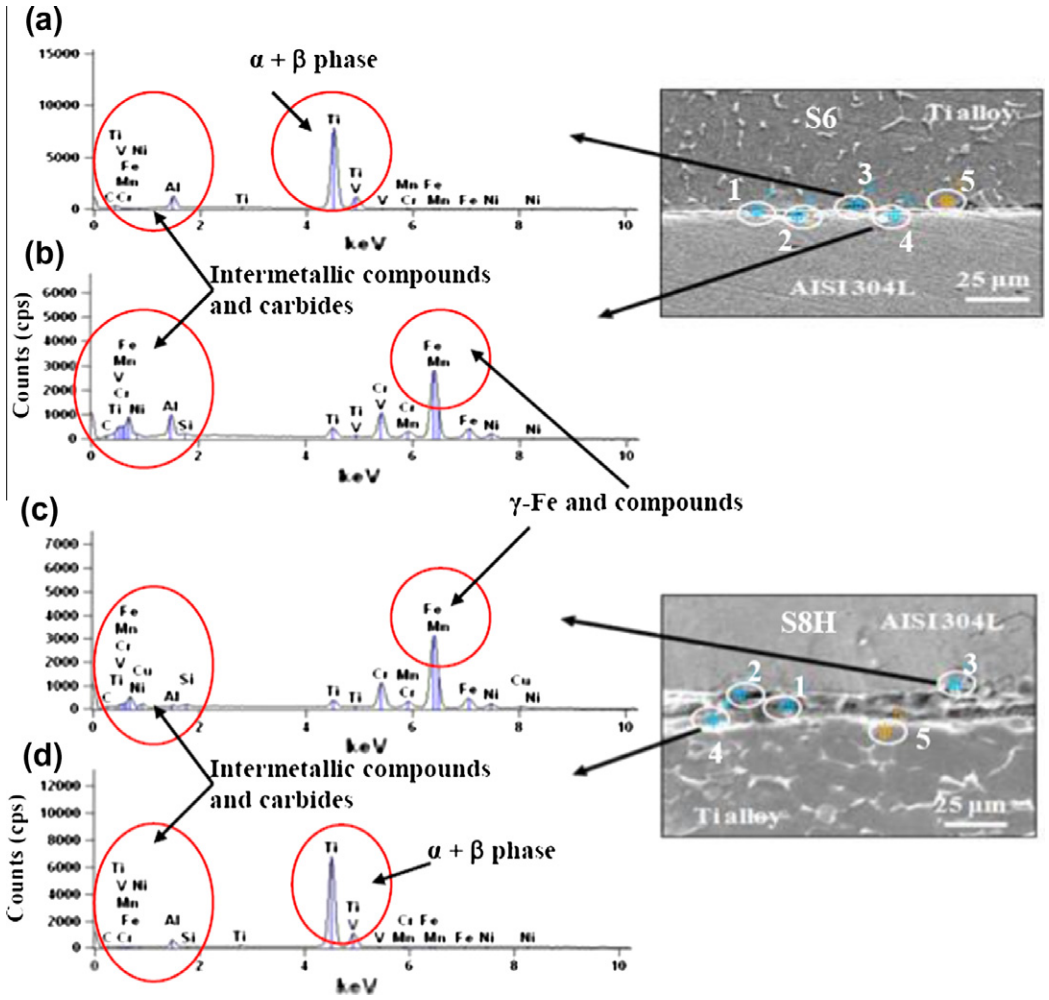

Fig. 8. The EDAX analysis: (a) Ti–6Al–4V side for the sample S6, (b) AISI 304L side for the sample S6, (c) AISI 304L side for the sample S8H and (d) Ti–6Al–4V side for the sample S8H.

Fig. 9a indicates the variation in the concentration of 'Fe', 'Cr', 'Ni' and 'Mn' in the base metal AISI 304L region close to the interface after DB for various processing temperatures. The concentration of 'Fe' decreases in the base metal AISI 304L (measured at a distance 4.5 μm from the interface) as the DB temperature rises from 875 to 950 °C (for samples S1, S4, S6 and S8), indicating an increase in the diffusion of 'Fe' into the Ti–6Al–4V. This result indicates that 'Fe' migrated from the AISI 304L to the Ti–6Al–4V side. The diffusivity of 'Fe', 'Cr', and 'Ni' increases in general with increases in temperature for samples that were not heat-treated. However, in the case of annealed samples, the 'Cr' concentration increases as the temperature increases at a distance of 4.5 μm from the interface on the AISI 304L side. This increase could be caused by the formation of intermetallic compounds and titanium carbides, which retard the diffusion of 'Fe' and 'Cr' to the Ti–6Al–4V side. Similarly, other elements, such as 'Ni' and 'Mn', diffuse in varying amounts, which are shown in Fig. 9a. The diffusion of elements such as 'Fe', 'Cr', and 'Si' into the Ti–6Al–4V stabilises the 'β' phase. In all samples (S1, S4, S6, and S8), the presence of increased amounts of the 'β' phase at the Ti–6Al–4V region is noted.

In the Ti–6Al–4V region close to the interface (shown in Fig. 9b), the concentration of dissolved 'Ti' decreases as the DB temperature rises from 875 to 950 °C for samples S1, S4, S6 and S8. The decrease in the percentage (measured at a distance 5 μm from the interface) of 'Ti' in the Ti–6Al–4V indicates an increase in its diffusion into AISI 304L because of the rise in the DB temperature. In addition, for the annealed samples S1H, S4H, S6H and S8H, the diffusivity of 'Ti' increases for all of the samples processed at higher temperatures. This increase indicates the migration of 'Ti' atoms towards the AISI 304L steel. The diffusivity of 'Ti' is greater than that of 'Fe' for various processing conditions. The other two alloying elements, 'Al' and 'V', diffuse into the AISI 304L regions; their concentration variation is shown in Fig. 9b. The diffusivity of 'V' is higher because it has greater affinity to form carbides. In addition, the diffusivity of 'Al' is greater than that of 'Fe', 'Mn', 'Ni', 'Ti' or 'V' (according to the diffusion coefficient values given in Table 4).

As shown in the Fig. 9c, the diffusion of 'Ti' into the AISI 304L side increases significantly in the annealed samples. This increase occurs because more TiC is formed during annealing. The formation of VC is more minimal in comparison to the formation of TiC. This process can be clearly observed in Fig. 9c. Similarly, as shown in Fig. 9d, the diffusion of 'Fe' and 'Cr' from the AISI 304L side to the Ti–6Al–4V is significant, particularly during the annealing heat treatment. The migration of 'Ti' to the AISI 304L side is greater than that of other elements, as shown in Fig. 9c and d. Because 'Fe' and 'Cr' are β-stabilizing elements, an increased amount of the stable 'β' phase is formed during the annealing heat treatment. This increase drives the formation of the cellular structure at the interface. In Fig. 9d, the diffusion of 'Fe', 'Cr', 'Ni' and 'Mn' into the Ti–6Al–4V region 5 μm from the interface is shown.

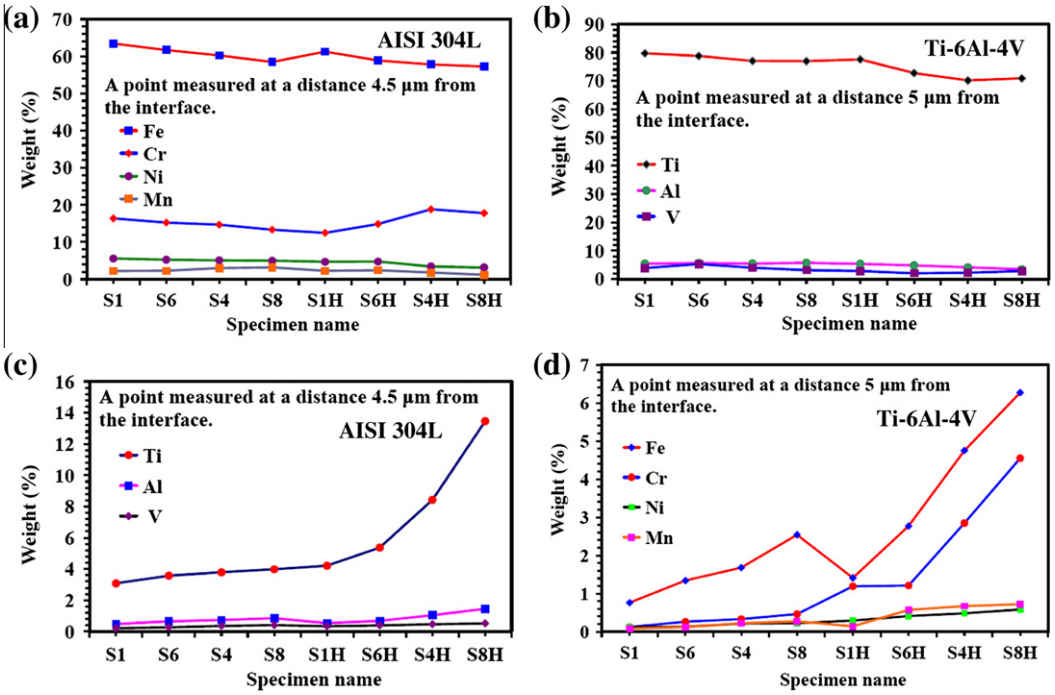

Fig. 9. Elemental concentration variation in: (a) AISI 304L side, (b) Ti–6Al–4V side, (c) diffusion of elements from Ti–6Al–4V to AISI 304L and (d) diffusion of elements from AISI 304L to Ti–6Al–4V.

As shown in Fig. 9d, the diffusivities of 'Mn' and 'Ni' marginally increase during the annealing heat treatment. This increase favours the formation of the cellular structure that is shown in Fig. 7d at the interface of sample S8H. In addition, the formation of increased amounts of TiC and reduced amount of VC favours the formation of this cellular structure. The whitish layer appears at the interface in Fig. 7d indicates the presence of an increased amount of TiC; the elevated TiC concentration may be the primary reason for the formation of the cellular structure. Qin et al. [40] has reported the diffusivity of elements such as 'Ti', 'Fe', 'Cr' and 'Ni' on either side of the joint; those results concur with the observations made in the present study.

3.4. Diffusion coefficients

Fick's second law for unidirectional flow under steady state conditions is given below.

$$\frac{\partial C}{\partial t} = \frac{\partial}{\partial x}\left(D\frac{\partial C}{\partial x}\right) \tag{1}$$

After measuring the concentration of an element (C_y) at a distance 'y' from the interface, Fick's second law can be rewritten as follows:

$$\frac{\partial C_y}{\partial t} = D\left(\frac{\partial^2 C_y}{\partial x^2}\right) \tag{2}$$

The above equation has the following solution:

$$C(y,t) = A - B\,erf\left(\frac{y}{2\sqrt{Dt}}\right) \tag{3}$$

$$A = \left(\frac{C_1 + C_2}{2}\right) B = \left(\frac{C_2 - C_1}{2}\right)$$

where C_1 and C_2 are the initial concentrations of the element under study in both materials, 'y' is the distance from the interface, 't' is the bonding time and 'D' is the diffusion coefficient [41]. The elemental concentration and distance from the interface on either side of the base metal has been measured using SEM and EDAX.

Table 4 shows that the diffusion coefficient values (D_{Ti}) for 'Ti' are greater than the values of D_{Fe}. This difference indicates that 'Ti' diffuses much faster than 'Fe' into AISI 304L. The intrinsic diffusion coefficients of 'Ti' ($D_{Ti} = 5.5 \times 10^{-14}$ m^2/s at 900 °C and $D_{Ti} = 9 \times 10^{-14}$ m^2/s at 800 °C) were reported by Kundu et al. [42]. In the current study, the obtained D_{Ti} values are less than the values reported in [42]. This difference could be attributed to the concentration difference in the composition of the base metals bonded in the present study and in the cited literature. The calculated D_{Fe} value of 5.52×10^{-16} m^2/s at 900 °C in the present work (refer Table 4, sample S6) is less than the diffusion coefficients for α-Fe ($D_{\alpha\text{-}Fe} = 5 \times 10^{-15}$ m^2/s at 900 °C) and greater than γ-Fe ($D_{\gamma\text{-}Fe} = 5 \times 10^{-17}$ m^2/s at 900 °C), as reported in the literature [42]. This difference is due to the increased diffusivity in 'β' titanium, which

Table 4
Diffusion coefficients (D) of various elements.

Sample name	Diffusion of elements into Ti–6Al–4V			Diffusion of elements into AISI 304L		
	D_{Fe}	D_{Mn}	D_{Ni}	D_{Ti}	D_{Al}	D_V
S1	3.85×10^{-16}	3.76×10^{-16}	3.14×10^{-16}	1.1×10^{-15}	–	6.77×10^{-14}
S6	5.52×10^{-16}	5.78×10^{-16}	6.41×10^{-16}	1.13×10^{-15}	–	7.38×10^{-16}
S5	5.46×10^{-16}	5.51×10^{-16}	3.70×10^{-16}	1.93×10^{-15}	1.99×10^{-15}	6.55×10^{-16}
S2	1.02×10^{-15}	8.46×10^{-16}	1.14×10^{-15}	3.08×10^{-15}	4.17×10^{-15}	2.69×10^{-15}

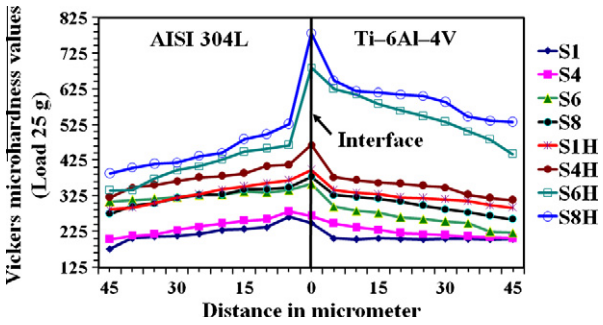

Fig. 10. Microhardness profile of the DB samples processed under various conditions.

has the body centred cubic structure. The calculated D_{Ni} values for all processing conditions are greater than the reported literature value, $D_{Ni} = 3 \times 10^{-17}$ m^2/s at 800 °C [42]. This difference shows that the increased bonding temperature increases the diffusion of 'Ni', leading to the greater D_{Ni} values obtained in the current work. Aleman et al. [43] reported that the D_{Ni} value in a Ti-alloy was 3×10^{-12} m^2/s at 900 °C, which is greater than the D_{Ni} value of 6.41×10^{-16} m^2/s obtained in the present work. The lower D_{Ni} values in the current work indicate that the concentration of 'Ni' in the base metal AISI 304L is only 8.38%, while in INCONEL 625 the 'Ni' content is approximately 63%. This result confirms that the diffusion of 'Ni' is concentration gradient oriented than chemical activation across the interface. The diffusivity of 'Ti' into the superalloy is slow ($D_{Ti} = 1.6 \times 10^{-17}$ m^2/s) in comparison to the D_{Ti} values given in Table 4. The slow diffusion could be caused by the presence of more amounts of alloying elements like 'Fe', 'Ni', 'Cr', 'Mo' and 'Mn' in the superalloy. The alloying elements present in the AISI 304L base metal is less which increase the diffusion of 'Ti'. The diffusion coefficients for D_{Mn}, D_{Al} and D_V are listed in Table 4.

3.5. Vickers microhardness

The microhardness values of the bonds were measured by applying a 25 g load in the transverse direction to the bond line. The distribution of the hardness values of the selective samples on either side of the centreline is shown as a graphical plot in Fig. 10. The minimum microhardness values were recorded for samples S1 and S1H. The increase in the hardness value is directly proportional to the increase in the temperature and time. The depth of diffusion and the amount of hard phase formation were reduced for samples S1, S4, S6 and S8 compared to S1H, S4H, S6H and S8H. The maximum hardness value of 378.6 VHN was recorded for the bonded sample S8. The hardness values in the present study were maximal at the interface and decreased as the distance from the interface on either side of the base metal increased which is in good agreement with the results reported in the literature [44]. A maximum value of 781 VHN was obtained for the annealed sample S8H. An increase in the width of the diffused region was observed with the rise in the hardness values across the interface as a result of the annealing heat treatment. The increases in the hardness values were directly proportional to the processing temperature and annealing heat treatment process. The DB of pure 'Ti' and precipitation hardened stainless steel performed by Poddar [45] at 1000 °C provided a maximum hardness value of ~750 VHN. In the present work, very high hardness values were recorded as a result of the formation of hard intermetallic compounds in sample S8H.

Table 5
Reaction products formed at the joint region.

Process parameters (°C/MPa/Min.)	Phase	'd' spacing	Structure
900, 4, 60 and annealed for 2 h.	Fe_2Ti	2.04510	Hexagonal
	Mn_2Ti	2.06416	Hexagonal
	$TiSi_2$	2.30190	Orthorhombic
	$AlNi_2Ti$	2.06475	Cubic
	Ni_4Ti_3	2.09200	Rhombohedral
	Fe_2Ti_4O	2.17661	Cubic
	Fe_2V_3	2.06475	Cubic
	$Fe_3Al_2Si_4$	2.01213	Orthorhombic
	Al_6Ti_{19}	2.20923	Hexagonal
	Al_4CrNi_{15}	2.05537	Cubic

3.6. X-ray diffraction (XRD)

In diffusion-bonded samples S1, S4, S6 and S8, the presence of the 'β' phase and intermetallic compounds such as the 'σ' phase, FeTi, Fe_2Ti, Mn_2Ti, Fe_2V_3, Ni_4Ti_3 and $TiNi_3$ were observed in the AISI 304L steel side. This observation is in good agreement with the literature [46]. In the Ti–6Al–4V region close to the interface, intermetallic compounds such as FeTi, Fe_2Ti, Fe_2V_3, TiV, Ti_3Al, TiNi, $TiNi_3$ and Ni_4Ti_3 were observed in annealed samples S1H, S4H, S6H and S8H. The XRD analysis performed on sample S6H indicated the presence of several intermetallic compounds at the joint region; the results are shown in Table 5. These compounds are hard and brittle, and they reduce the tensile strength of the annealed DB samples processed at higher temperatures. Increased amounts of ternary phases, such as $AlNi_2Ti$, $Fe_3Al_2Si_4$, Al_4CrNi_{15} and Fe_2Ti_4O (see Table 5), are observed in the annealed samples compared to the non-heat-treated samples. In the literature, the formation of TiAl, Ti_3Al, TiNi, $TiNi_2$ and $TiNi_3$ is reported [46,47]. In addition, phases such as Ni_4Ti_3 and small quantities of Al_6Ti_{19} are identified from the XRD analysis in the present work. In the annealed DB samples, oxides are present at the joint region (Table 5). Their presence could be caused by the failure of the vacuum environment inside the furnace during the annealing process.

The XRD pattern obtained for the Ti–6Al–4V side of the fractured surface of sample S1 (shown in Fig. 11a) reveals the presence of the 'β' phase, Fe_2Ti, $TiNi_2$, Fe_2Ti_4O and Ni_4Ti_3. The XRD analysis of the fractured surface of sample S4 indicates formation of increased amounts of the 'β' phase and intermetallic compounds, such as Fe_2Ti, $TiNi_2$, Fe_2Ti_4O and Ti_3Ni_4. The depth of diffusion and formation of intermetallic compounds are directly proportional to the bonding temperature. The XRD analysis conducted at the fracture site for the annealed sample S6H (shown in Fig. 11a) indicates an increased number of peaks and counts. This result indicates the diffusion of β-stabilising elements, such as 'Fe', 'Cr', and 'Si', to form the 'β' phase and intermetallic compounds at the fracture site. In addition, the diffusion of 'Ni' into Ti–6Al–4V caused the formation of compounds $TiNi_2$ and Ni_4Ti_3. Furthermore, oxides are present at the fracture site (shown in Fig. 11a). On the AISI 304L side of sample S1 (shown in Fig. 11b), the XRD pattern reveals the presence of Fe_2Ti, Ni_4Ti_3, $TiNi_3$, Fe_2Ti_4O, the 'σ' phase and γ-Fe. The presence of 'Fe', 'Ni', 'Cr', 'C' and 'O' indicates the formation of intermetallic compounds, carbides and oxides in the joint region. The XRD analysis of sample S4 indicates a slight increase in the diffusion of the above elements. The amount of intermetallic compounds formed increased because of the increase in the DB temperature. This result is in good agreement with other reported work [46,47]. The XRD analysis at the fractured region of annealed sample S6H indicates the formation of an increased amount of intermetallic compounds and oxides in comparison to the DB samples S1 and S4. The annealing heat treatment performed on the DB samples increases the amounts of binary and ternary intermetallic compounds formed,

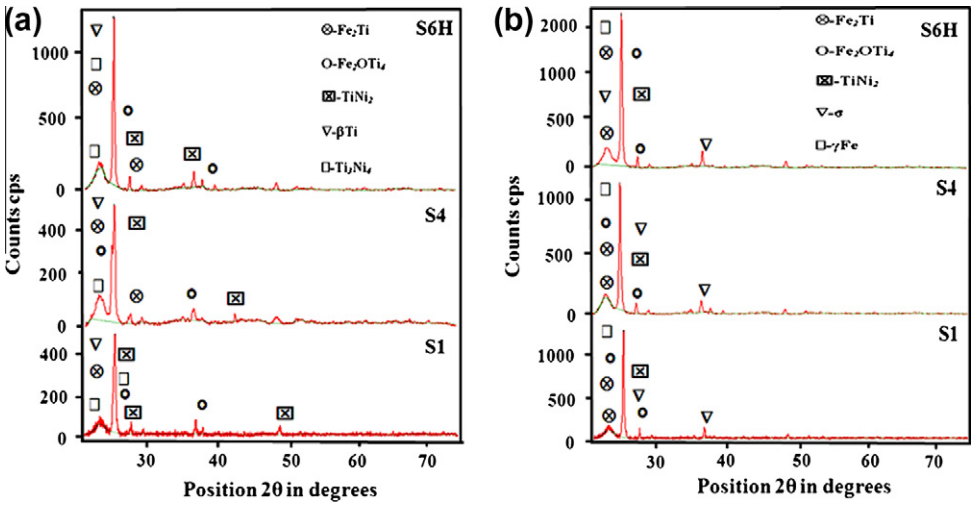

Fig. 11. XRD pattern of the fractured surfaces: (a) Ti–6Al–4V side, (b) AISI 304L side.

which reduces the diffusivity of various elements because the transformed compounds prevent further diffusion.

3.7. Tensile strength

The average tensile strengths of the samples processed at various temperatures and conditions are shown in Table 6. For the DB samples S1 and S8H, minimum tensile strengths of 98.3 and 96.5 MPa, respectively, were obtained. The poor strength exhibited by sample S1 is attributed to the lack of diffusion because of insufficient bonding time and poor contact between the adjacent surfaces. For the annealed sample S8H, the poor strength is caused by the formation and growth of hard and brittle intermetallic compounds in the joint region. A maximum tensile strength of 144.7 MPa was obtained for the as-bonded sample S6. Table 6 shows that the bonded samples with no annealing had low strength compared to the samples subjected to annealing after diffusion bonding. The maximum tensile strength of 242.6 MPa was observed for the annealed DB sample S6H. During annealing, diffusion induced voids formed at the interface, which decreased the tensile strength relative to that of the unannealed DB samples (example S8H).

Similarly, at the lower processing temperature of 875 °C, the annealed sample S1H had an average tensile strength value of 214.4 MPa (shown in Table 6). These observations indicate that good bond strength is exhibited by the samples processed between 875 and 900 °C at pressures 4 to 8 MPa and a bonding time of 60 min, with an annealing heat treatment applied for 2 h. In addition, the strength of the joints is related to the size factor and specimen geometry. The DB samples produced with no annealing heat treatment exhibited poor strength. After annealing, the average tensile strength of the joint increased. The narrower rectangular specimens, which had dimensions of $40 \times 18 \times 16$ mm, exhibited more strength than the wider square specimens with dimensions of 40×40 v 16 mm. The above observations indicate that annealing is essential for large samples. Moreover, the surface finish must be flat to obtain the best possible average tensile strength in the bonded samples. At room temperature, the base metal AISI 304L experiences more plastic deformation than Ti–6Al–4V. Very high pressure applied to the base metals under cold working conditions increases their surface contact. Uneven contact between the mating parts leads to uneven diffusion and thickness variation in the diffused region (example S1). This factor reduces the average tensile strength of the joints at lower bonding temperatures and times. Additionally, at higher temperatures, localised diffusion occurred, and more hard intermetallics of high thickness were formed, resulting in a reduction of the average tensile strength of the joints (sample S8 in Table 6). To obtain uniform thickness at the interface, the joints were plastically deformed at 750 °C by applying impulse pressure. This process increased the average tensile strength of the joints. The maximum tensile strength obtained in the present study is comparable with the maximum value obtained in the previous work performed by Sheng et al. [48].

3.8. Fracture surface

The fractured surfaces of the tensile test samples were examined with SEM. All of the tensile test samples failed at the interface and exhibited a brittle mode of fracture. The processing temperature

Table 6
The tensile strength of the diffusion bonded joints.

Specimen name	Process parameters (°C/MPa/Min.)	Average tensile strength (MPa)	Heat treated specimen name	Average tensile strength (MPa)
S1	875, 8, 60	98.3	S1H	214.4
S2	950, 4, 60	132.4	S2H	108.6
S3	900, 8, 60	122.6	S3H	221.7
S4	925, 4, 60	138.2	S4H	219.5
S5	925, 8, 60	106.4	S5H	170.3
S6	900, 4, 60	144.7	S6H	242.6
S7	875, 4, 60	114.6	S7H	204.5
S8	950, 8, 60	108.3	S8H	96.3

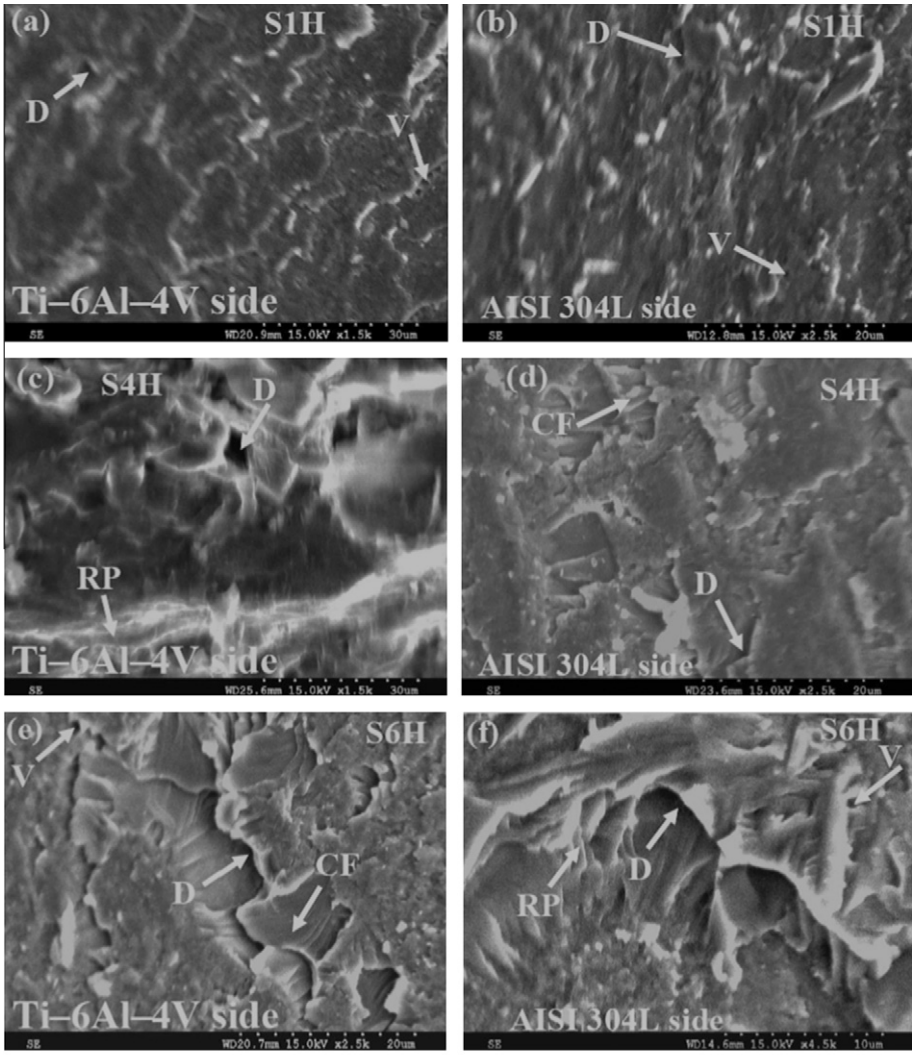

Note: CF-Cleavage fracture, V-Voids, D-Dimples, RP-River Pattern.

Fig. 12. SEM fractographs: (a) S1H, Ti–6Al–4V side, (b) S1H, AISI 304L side, (c) S4H, Ti–6Al–4V side, (d) S4H, AISI 304L side, (e) S6H, Ti–6Al–4V and (f) S6H, AISI 304L side.

dependent formation of hard and brittle intermetallic compounds in varying amounts may have caused the samples to fail in this way. On the fractured surface of sample S1H, shown in Fig. 12a, one or two dimples (marked 'D') are present on the Ti–6Al–4V side. In addition, several voids (marked 'V') are observed close to the grain boundary. These voids developed because of the lack of diffusion of atoms from the matrix in that region to the other side of the joint. The presence of voids and cleavage fractures indicates that the mode of fracture is brittle in nature. The SEM image shown in Fig. 12b, of the AISI 304L side, reveals the presence of few dimples and voids at the fractured site, indicating that the mode of fracture is brittle. Here, an increased number of voids and dimples formed in comparison to the Ti–6Al–4V side.

The fractograph of sample S4H in the Ti–6Al–4V region, shown in Fig. 12c, reveals a brittle mode of fracture. In the fracture at the interface region, point 'D' indicates the presence of large dimples and a river pattern (marked as 'RP'), indicating a cleavage fracture. In addition, Fig. 12d, which was taken at the AISI 304L side, exhibits large dimples and cleavage fracture ('CF') sites. Sample S4H exhibited higher tensile strength than sample S1H because of the presence of large dimples and 'CF' sites. In Fig. 12e, at the Ti–6Al–4V side, very large dimples occurred. The presence of these dimples may explain the increased tensile strength exhibited by this sample (S6H). The increased percentage of 'CF' sites indicates a brittle mode of fracture. Cleavage fracture sites were noted in the referred literature [48,49]. The SEM image (AISI 304L side) shown in Fig. 12f reveals large dimples and an 'RP' along with 'CF' sites. The fracture patterns observed in this study are in good agreement with those observed in the referred works [48,49]. In addition, the fracture mode exhibited in the reported work by Elrefaey and Tillmann [50] is in agreement with the observations of the present work.

4. Conclusions

Under the investigated conditions, DB samples processed at a temperature of 900 °C and a holding pressure of 4 MPa for 60 min, followed by annealing, exhibited a maximum tensile strength of 242.6 MPa. The DB samples possessed tensile strengths that were 41.6% and 25.3% of the base metals, AISI 304L and Ti–6Al–4V, respectively. A maximum hardness value of 781 VHN was obtained for the DB samples processed at 950 °C and annealed for 2 h. The increase in hardness is due to the formation of hard and brittle intermetallic compounds at higher temperatures. The decrease in mechanical properties is attributed to the higher rate of phase transformation and the development of new phases at

higher bonding temperatures. The estimated diffusion coefficient values indicate that the diffusivity of 'Ti is higher than 'Fe'. The EDAX and XRD analyses of the DB samples confirmed the presence of compounds such as Fe_2Ti, Mn_2Ti, $TiNi_2$, Ti_2Si_2, Fe_2V_3, Ti_3Ni_4, $Fe_3Al_2Si_4$, Al_6Ti_{19}, Al_4CrNi_{15} and Fe_2Ti_4O. These phases were observed to impair the mechanical properties of the DB samples at higher bonding temperatures.

Acknowledgements

The authors kindly acknowledge the financial support provided by (Grant No. 8023/BOR/RID/RPS-134/2007-2008) All India Council for Technical Education (AICTE), New Delhi, India. We express our wholehearted gratitude to the management of our institution.

References

[1] Atasoy E, Kahraman N. Diffusion bonding of commercially pure titanium to low carbon steel using a silver interlayer. Mater Charact 2008;59:1481–90.
[2] Vigraman T, Narayanasamy R, Ravindran D. Microstructure and mechanical property evaluation of diffusion-bonded joints made between SAE 2205 steel and AISI 1035 steel. Mater Design 2012;35:156–9.
[3] Vigraman T, Ravindran D, Narayanasamy R. Diffusion bonding of AISI 304L steel to low carbon steel with AISI 304L steel interlayer. Mater Design 2012;34:594–602.
[4] Lee HS, Yoon JH, Park CH, Ko YG, Shin DH, Lee CS. A study on diffusion bonding of superplastic Ti–6Al–4V ELI grade. J Mater Proc Technol 2007;187–188:526–9.
[5] Lee HS, Yoon JH, Yi YM. Fabrication of titanium parts by massive diffusion bonding. J Mater Proc Technol 2008;201:280–4.
[6] Xun YW, Tan MJ. Applications of superplastic forming and diffusion bonding to hollow engine blades. J Mater Proc Technol 2000;99:80–5.
[7] Salishchev GA, Galeyev RM, Valiakhmetov OR, Safiullin RV, Lutfullin RY, Senkov ON, et al. Development of Ti–6l–4V sheet with low temperature superplastic properties. J Mater Proc Technol 2001;116:265–8.
[8] Koike J, Shimoyama Y, Ohnuma I, Okamura T, Kainuma R, Ishida K, et al. Stress–induced phase transformation during superplastic deformation in two phase Ti–Al–Fe alloy. Acta Mater 2000;48:2059–69.
[9] Wei Y, Aiping W, Guisheng Z, Jialie R. Formation process of the bonding joint in Ti/Al diffusion bonding. Mater Sci Eng A 2008;480:456–63.
[10] Duarte LI, Ramos AS, Vieira MF, Viana F, Vieira MT, Kocak M. Solid state diffusion bonding of gamma-TiAl alloys using Ti/Al thin films as interlayers. Intermetallics 2006;14:1151–6.
[11] He P, Feng JC, Zhang BG, Qian YY. A new technology for diffusion bonding intermetallic TiAl to steel with composite barrier layers. Mater Charact 2003;50:87–92.
[12] Konga F, Chena Y, Zhang D. Interfacial microstructure and shear strength of Ti–6Al–4V/TiAl laminate composite sheet fabricated by hot packed rolling. Mater Design 2011;32:3167–72.
[13] Kundu S, Gosh M, Chatterjee S. Reactive diffusion bonding between commercially pure titanium and stainless steel using nickel interlayer. ISIJ Int 2004;44:1882–7.
[14] Kundu S, Chatterjee S. Interfacial microstructure and mechanical properties of diffusion bonded titanium-stainless steel joints using a nickel interlayer. Mater Sci Eng A 2006;425:107–13.
[15] Torun O, Celikyurek I. Boriding of diffusion-bonded joints of pure nickel to commercially pure titanium. Mater Design 2009;30:1830–4.
[16] Yan JC, Zhao DS, Wang CW, Wang LY, Wang Y, Yang SQ. Vacuum hot roll bonding of titanium and stainless steel using nickel interlayer. Mater Sci Technol 2009;25:914–8.
[17] He P, Yue X, Zhang JH. Hot pressing diffusion bonding of a titanium alloy to a stainless steel with an aluminium alloy interlayer. Mater Sci Eng A 2008;486:171–6.
[18] Kundu S, Chatterjee S. Evolution of interface microstructure and mechanical properties of titanium/304 stainless steel diffusion bonded joint using Nb interlayer. ISIJ Int 2010;50:1460–5.
[19] Yuan XJ, Sheng GM, Qin B, Huang WZ, Zhou B. Impulse pressuring diffusion bonding of titanium alloy to stainless steel. Mater Charact 2008;59:930–6.
[20] Ze–bao L, Liang W, Xu–hu Z. HIP diffusion bonding of P/M titanium alloy Ti-6Al-4V and stainless steel 1Cr18Ni9Ti. Trans Nonferrous Met Soc China 2007;17:s79–83.
[21] Annual book of ASTM standards, Standard test methods for tension testing of metallic materials [Metric], ASTM Hand Book, vol. 03.01 West Conshohocken; 2002. p. 82–91.
[22] Tan MJ, Chen GW, Thiruvarudchelvan S. High temperature deformation in Ti–5Al–2.5Sn alloy. J Mater Proc Technol 2007;192–3:434–8.
[23] Wang GC, Fu MW. Maximum m superplasticity deformation for Ti–6Al–4V titanium alloy. J Mater Proc Technol 2007;192–193:555–60.
[24] Kim JS, Kim JH, Lee YT, Park CG, Lee CS. Microstructural analysis on boundary sliding and its accommodation mode during superplastic deformation of Ti–6Al–4V alloy. Mater Sci Eng A 1999;263:272–80.
[25] Kundu S, Chatterjee S. Diffusion bonding between commercially pure titanium and micro-duplex stainless steel. Mater Sci Eng A 2008;480:316–22.
[26] Yang KL, Huang JC, Wang YN. Phase transformation in the β phase of super α2 Ti3Al base alloys during static annealing and superplastic deformation at 700–1000 °C. Acta Mater 2003;51:2577–94.
[27] Park CH, Ko YG, Park JW, Lee CS. Enhanced superplasticity utilizing dynamic globularization of Ti–6Al–4V alloy. Mater Sci Eng A 2008;496:150–8.
[28] Kundu S, Ghosh M, Laik A, Bhanumurthy K, Kale GB, Chatterjee S. Diffusion bonding of commercially pure titanium to 304 stainless steel using copper interlayer. Mater Sci Eng A 2005;407:154–60.
[29] Salishchev GA, Imayev RM, Senkov ON, Imayev VM, Gabdullin NK, Shagiev MR, et al. Formation of a submicrocrystalline structure in TiAl and Ti3Al intermetallics by hot working. Mater Sci Eng A 2000;286:236–43.
[30] Liauo CS, Fu HC, Hsiao ic, Huang JC. On the β-transus and order/disorder transition temperature in superplastic super α2 Ti3Al base alloy. Mater Sci Eng A 1999; 271:275-85.
[31] Feng WX, Ma Mo, Xue-Bin L, Xue-Qing WU, Chao-Gui T, Rong-Kai S, et al. Diffusion bonding of γ TiAl alloy to Ti–6A1–4V alloy under hot pressure. Trans Nonferrous Met Soc China 2006;16:1059–63.
[32] Gammon LM, Briggs RD, Packard JM, Batson KW, Boyer R, Domby CW. In: Metallography and microstructures of titanium and its alloys, metallography and microstructures, vol. 9, ASM Handbook, ASM International; 2004. p. 2157–207.
[33] Ducki KJ. Precipitation and growth of intermetallic phase in a high temperature Fe–Ni alloy. J Achieve Mater Manu Eng 2006;18:87–90.
[34] Todd RI, Hodges CS, Wong YC, Wang ZC, Ridley N. Objective modeling of diffusion bonding in superplastic duplex stainless steels. Mater Sci Forum 1997;243–245:675–80.
[35] Voort VGF, Lucas GM, Manilova EP. In: Metallography and microstructures of stainless steels and maraging steels, metallography and microstructures, vol. 9, ASM Handbook, ASM International; 2004. p. 1590–666.
[36] Murray JL. In: Baker H, Okamoto H, editors. Alloy phase diagrams, vol. 3, ASM Hand Book, ASM International; 2004. p. 709–869.
[37] Ferrante M, Pigoretti EV. Diffusion bonding of Ti–6Al–4V to AISI 316L stainless steel: mechanical resistance and interface microstructure. J Mater Sci 2002;37:2825–33.
[38] Ghosh M, Chatterjee S, Mishra B. The effect of intermetallics on the strength properties of diffusion bonds formed between Ti–5.5Al–2.4V and 304 stainless steel. Mater Sci Eng A 2003;363:268–74.
[39] Murray JL. In: Baker H, Okamoto H, editors. Alloy phase diagrams, vol. 3. ASM Hand Book, ASM International; 2004. p. 327–1421.
[40] Qin B, Sheng GM, Huang JW, Zhou B, Qiu SY, Li C. Phase transformation diffusion bonding of titanium alloy with stainless steel. Mater Charact 2006;56:32–8.
[41] Raghavan V. Mater. Sci. Eng. New Delhi: Prentice Hall India Ltd.; 2004. p. 178–200.
[42] Kundu S, Chatterjee S. Structure and properties of diffusion bonded transition joints between commercially pure titanium and type 304 stainless steel using a nickel interlayer. J Mater Sci 2007;42:7906–12.
[43] Aleman B, Gutierrez I, Urcola JJ. Interface microstructures in the diffusion bonding of a titanium alloy Ti 6242 to an INCONEL 625. Metall Mater Trans A 1995;26A:437–46.
[44] Mudali UK, Rao BMA, Shanmugam K, Natarajan R, Raj B. Corrosion and microstructural aspects of dissimilar joints of titanium and type 304L stainless steel. J Nucl Mater 2003;321:40–8.
[45] Poddar D. Solid state diffusion bonding of commercially pure titanium and precipitation hardening stainless steel. Int J Recent Trends Eng May 2009;5:93–9.
[46] Shyu JS, Chuang TH. Diffusion bonding/superplastic forming of Ti–6Al–4V–2Sn/SUS 304 stainless steel/Ti–6Al–4V–2Sn. J Mater Eng Per 1996;5:84–8.
[47] Kundu S, Ghosh M, Chatterjee S. Diffusion bonding of commercially pure titanium and 17–4 precipitation hardening stainless steel. Mater Sci Eng A 2006;428:18–23.
[48] Sheng GM, Huang JW, Qin B, Zhou B, Qiu SY, Li C. An experimental investigation of phase transformation superplastic diffusion bonding of titanium alloy to stainless steel. J Mater Sci 2005;40:6385–90.
[49] Kundu S, Sam S, Chatterjee S. Interface microstructure and strength properties of Ti–6Al–4V and microduplex stainless steel diffusion-bonded joints. Mater Design 2011;32:2997–3003.
[50] Elrefaey A, Tillmann W. Solid state diffusion bonding of titanium to steel using a copper base alloy as interlayer. J Mater Proc Technol 2009;5:2746–52.